THE CMC THERMAL PROTECTION SYSTEM OF THE ATHEAT HYPERSONIC VEHICLE

T. Reimer¹, G. Di Martino¹, C. Rauh¹, L. Baier¹, I. Petkov¹, D. Hargarten², T. Ecker³, A. Gülhan⁴

¹German Aerospace Center (DLR), Institute of Structures and Design, 70569 Stuttgart, Germany
²German Aerospace Center, DLR, Space Operations and Astronaut Training, 82234 Oberpfaffenhofen-Weßling, Germany
³German Aerospace Center, (DLR), Institute of Aerodynamics and Flow Technology, 37073 Göttingen, Germany
⁴German Aerospace Center, (DLR), Institute of Aerodynamics and Flow Technology, 51147 Cologne, Germany

ABSTRACT

The German Aerospace Center (DLR) carries out a flight research program focused on developing technologies for RLV systems which is based on sounding rocket flights carrying experimental vehicles. The objective for ATHEAt is to increase the Mach number and the duration of flight at high Mach number further. The TPS design of the ATHEAt vehicle will feature new developments, both in terms of the structure manufacturing and the TPS design. Specifically, there are four moveable flaps integrated into the TPS. In addition to the function of protecting the vehicle from the environment, the TPS elements also serve as carrier structures for a large number of sensors to collect the flight data. The paper will give an overview about the design and the development of the TPS elements.

Index Terms—TPS, hypersonic, CMC, sounding rocket

1. INTRODUCTION

Sustainable access to space via reusable launch vehicles (RLV) is the principal objective in the launcher development, in particular also in the national German space transportation strategy. A robust and reliable design requires validation data. DLR is supporting this strategy via a two-fold approach. First, a wide range of ground testing facilities are operated to replicate the flight environment. However, since ground test facilities are limited in duplicating the flight conditions, ground testing is complemented by flight experiments using scaled vehicles to close the gap. Since the shortcomings of design tools are mostly found in the modelling of high temperature gas phenomena and gas surface interaction in a hypersonic environment, these are the targeted conditions in flight. To this aim, a dedicated flight research program is carried out which is focused on advancing the technologies for RLV in hypersonic flight. The program is based on sounding rocket flights carrying experimental vehicles flying at high Mach number to collect the relevant flight data. Past flights within this program included the SHEFEX flights.



Figure 1 The SHEFEX II flight experiment.

Due to launcher limitations, the SHEFEX I flight experiment reached no higher velocity than Mach 6 [1]. The SHEFEX II flight experiment [2], shown in Figure 1, went up to Mach 10, however, the phase of high aerothermal load was restricted to less than 30 seconds. As a consequence, for the STORT flight experiment, shown in Figure 2, it was decided to use a three-stage sounding rocket configuration and to fly a so-called suppressed trajectory with a relatively low apogee height of 38 km. Thereby it was possible to increase the integral heat load on the vehicle structures and to achieve one and a half minutes of almost constant Mach 8 velocity [3].



Figure 2 The STORT flight experiment.

The ATHEAt flight experiment will take this approach further and is aiming at an even higher Mach number for an extended duration of time. The goal is to reach a peak speed of Mach 10 which will be followed by a flight of three minutes duration at a velocity of over Mach 8. The launch vehicle will be a two-stage sounding rocket with the Red Kite motor as first stage and a Black Brant IV as second stage. The payload forebody requires a thermal protection system (TPS) because the aerothermal heat load is considerable. With regard to the preceding experimental flights, the TPS design in ATHEAt incorporates major advancements which will be detailed in the following. In addition, also with regard to the collection of flight data, an effort was made to increase both the number of sensors on the vehicle and the quality of the data.

2. DESIGN CONCEPT OF THE TPS

The design concept for the ATHEAt TPS is guided by the following considerations. The TPS baseline concept is an aeroshell made of rigid ceramic matrix composite (CMC) structures which are attached to the vehicle airframe by dedicated attachment components to transfer the mechanical loads, as in principle shown in Figure 3. The design is based on the experience from the STORT project [4, 5]. The space between the metallic airframe and the CMC surface structures is filled with a high-temperature insulation. As the TPS components are made from CMC material, the manufacturing capabilities and restrictions need to be taken into account. The vehicle is divided into several sections, named as the segments, taking into account the size limitations of the material production and practical aspects of vehicle assembly.

The shape of the vehicle contour is based on aerodynamic considerations. For the tip and the segments A to B it is similar to the one of STORT, which was an ogive with a spherical tip of very small radius. For the ATHEAt vehicle, one major change in the vehicle shape, impacting the TPS design, was the introduction of flaps as aerodynamic control

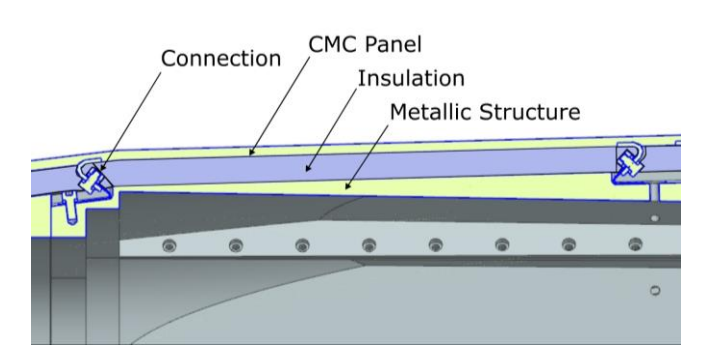


Figure 3 Schematic of the TPS design.

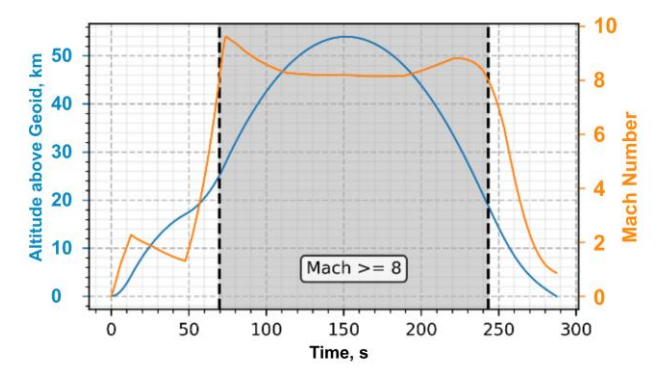


Figure 4 ATHEAt Trajectory.

surfaces. As the flaps are planar components and because they shall be integrated nicely into the vehicle shape, it was decided to modify the vehicle contour from a circular cross section in the front of the vehicle to an octagonal shape where the flaps are located. Therefore, four larger sides are present where the flaps are positioned and four smaller sides between each flap.

Due to this shape change from a circular to a cornered cross section, the wet filament winding technology was complemented by the production of individual CMC shell structures of various shapes. Whereas the wet filament winding technology is used to produce one closed axially symmetric structure, several of the shells are used to build the TPS of one segment. The shell structures include types which feature only curved surfaces, then there are types that have only planar areas and there are mixed types which consist of curved surfaces and planar areas.

3. AEROTHERMAL ENVIRONMENT

The trajectory features an apogee of approximately 54 km and an impact ground range of approximately 530 km. This requires the use of a low launching elevation angle as well as a coast phase following the first stage burnout to allow for the gravity turn to reduce the trajectory angle. To reduce the influence of wind and other factors that are difficult to correct before launch, the second stage ignition time is determined on board, based on an actual trajectory prediction using a 3DoF in-flight flight dynamic simulation. The resulting flight profile is shown in Figure 4. Based on the predictions, a Mach number between 8 and 10 can be achieved for roughly 170 seconds. The maximum predicted Mach number is 9.6 [6].

4. TPS ELEMENTS

The vehicle forebody is divided into six sections in terms of the fiber ceramic TPS as shown in Figure 5. At the very front is the tip, which is followed by the segments A to D and F.

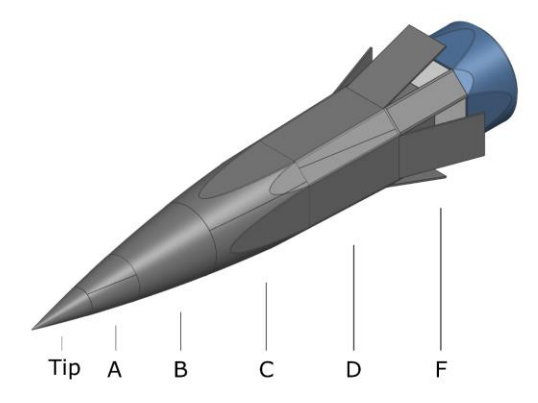


Figure 5 The ATHEAt forebody.

Whereas the segments A and B have a curved surface, segment C is a combination of curved and planar surfaces to achieve the change. Segment D has only planar surfaces to provide for a clean and undisturbed inflow to the flaps that are located in segment F. After the flap module, a transition module provides for the mechanical connection to the downstream service modules of the overall payload.

4.1 Tip

The forebody tip is a solid body made from one piece of C/C-SiC material. The reason is, that the solid body design provides for a heat sink that helps in controlling the temperature in the front of the vehicle. There are sensors embedded which are limited in terms of use temperature. In addition this helps to control the temperatures at the mechanical connection between the CMC tip and the metallic structure of segment A.

4.2 Segment A

In segment A four individual CMC shells are located. The reason is, that there are hoist points foreseen that should be accessible until late during the assembly, as displayed in Figure 6. Therefore, the parts covering the hoist points shall be assembled late during the overall assembly process, resulting in the decision to have four parts in total, of which two are assembled early in the process and two late to cover the hoist points. The requirement to install the remaining two cover shells late when the forebody is already completely assembled necessitated the design of a special attachment system that works without having access to it.



Figure 6 Handling points in segment A.

The other two parts which are assembled earlier feature the proven double-l connection system used already on STORT.

4.3 Segment B

In segment B a circumferentially closed CMC shell produced by wet filament winding technology is foreseen which is shown in Figure 12 a). Here, the proven design of the STORT TPS is used with the double-l connections in a circular arrangement at both ends; shown in Figure 12 b).

4.4 Segment C

They feature a transition from a circular cross section to an octagonal cross section as presented in Figure 7. In the front of the segment C parts, the shape is the double-curvature contour of the ogive. Further downstream, the shape is intersected with planar areas that extend from the flaps upstream, cutting away the curvature in order to have the planar surfaces in front of the flaps. Also in these structures, the proven double-l connections are used at the front and back end to affix it to the metallic structure.

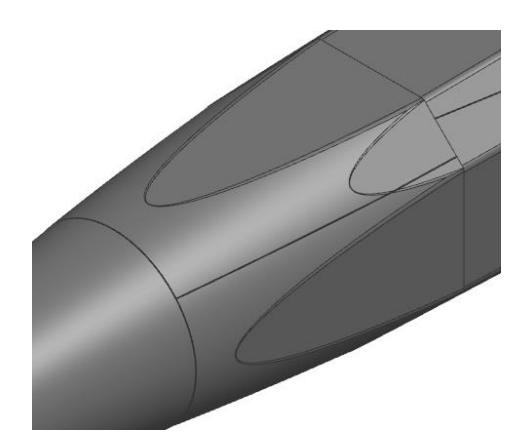


Figure 7 Segment C structures of the forebody.

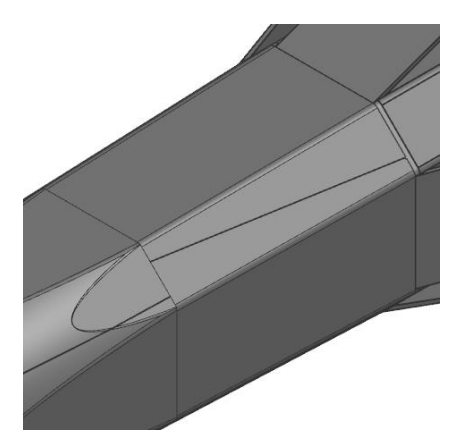


Figure 8 Segment D structures of the forebody.

4.5 Segment D

The CMC structures in segment D, shown in Figure 8, consist of only planar surfaces. Each component has a large flat part and two smaller "wings" covering the smaller areas of the octagon. The intersection lines between each of the four segment D parts are inclined with regard to the streamline of the flow, resulting in a part geometry with different front end and back end widths. The segment D structures incorporate two active cooling experiments. They are located on opposite sides of the vehicle, one featuring transpiration cooling, the other using impingement cooling, both using gas as the coolant medium.

4.6 Segment F

On the last segment of the CMC forebody, four flaps are located as indicated in Figure 9. They serve as aerodynamic experiments to investigate typical control surfaces to be applied in hypersonic flight. In addition, they are an engineering experiment to investigate the design and manufacturing issues that come along with such a mechanical system. The flap system parts are almost completely made from CMC material, except for bearing components in the front hinge line and at the actuator hinge inside the vehicle. In the center of the flap, on the leeward face, a hot bearing is situated where the drive rod contacts the flap. The flaps are fully functional, including an actuator system driven by compressed gas to move them. However, since the vehicle has no flight control system, the flaps are stowed initially and will only be deployed outward into the flow once when the vehicle is in the apogee and then remain in a fixed deployed position. The flaps and their surroundings are instrumented with a large number of different sensors to collect the data concerning the flowfield around the flaps.

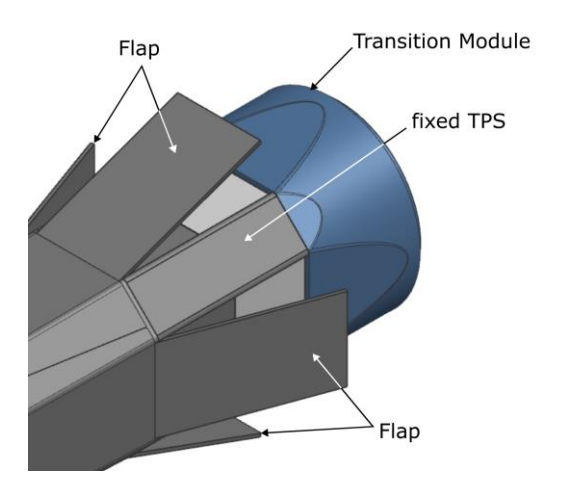


Figure 9 Flap structures of the forebody.

6. CMC PART MANUFACTURING

The manufacturing of the C/C-SiC components for the ATHEAt vehicle is a demanding process. It is built on established processing technology but also new production technology was developed and transferred into actual hardware processing. The Liquid Silicon Infiltration (LSI) process is used here to manufacture the C/C-SiC components. This process has already been described [7] and is well established. In short, it is a three-step process starting from a CFRP component, which is pyrolyzed to a C/C part, which in turn is finally processed to become C/C-SiC. The last



Figure 10 The ATHEAt C/C-SiC tip.

processing step is a reaction melt infiltration (RMI) process during which liquid silicon is infiltrated into the open porosity of the C/C material. In this process, the liquid silicon reacts insitu with the preform carbon to form silicon carbide.

As the TPS aeroshell is a segmented design, consisting of elements of varying shapes, different part shaping technologies were used following a nearnet-shape approach. Four main variants in the shaping method can be identified:

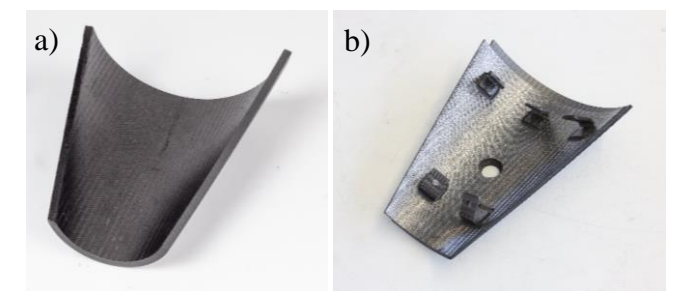


Figure 11 Segment A C/C part as fired (a) and machined with l-brackets joined (b).

- Machining from a solid block as for the tip.
- Non-planar shells made in net-shape via autoclave processing as for segments A, C and D parts.
- Closed shell in net-shape via wet filament winding as for segment B.
- Flat plates as for the flap elements via autoclave processing.

For the tip, a plate of large thickness was produced and the component was milled out of a solid block of C/C-SiC directly to the final contour, shown in Figure 10.

For the parts of segment A, C and D, there was the common task to account for the processing effects on the part geometry, as the goal is to produce the components in a net-shape condition without further machining of the surface contour. The parts that pose the greatest difficulty are the non-planar shells of segment C, shown in Figure 13; that combined a double-curvature contour (which is present also in the segment A parts) with planar areas at different angles (which is present also in the segment D parts). The difficulty is to ensure a correct geometry after the material processing because the material undergoes major changes due to the effect of the matrix shrinkage during pyrolysis. For flat plates, there is basically just a thickness decrease as a result, whereas in the case of a non-planar geometry with curvature, the shape change is not trivial.

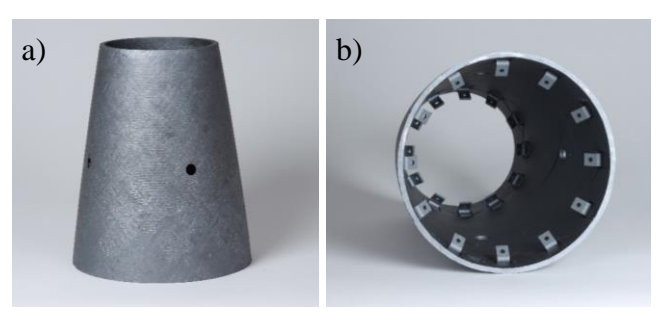


Figure 12 The C/C-SiC part of segment B as finally machined; outside view (a) and internal view with joined l-brackets (b).



Figure 13 Segment C part in C/C condition.

A numerical simulation method was employed to account for the effect and to design the moulds for the components accordingly. The method proved to be efficient and the parts could be used without further machining of the surface contour as it was intended.

In the case of the segment B component, which was produced via the wet filament winding process, there were major process improvements implemented in comparison to the approach used for the STORT parts. The process enhancements led to significantly improved component quality. The component is practically free of internal defects which are hard to control in wet filament winding. The component was produced with a small amount of extra material on the outward surface to machine the outer contour to the final shape in the C/C-SiC condition.

On all the CMC components except for the tip, the in-situ joining method [8] was applied to affix CMC brackets to the shells to apply the double-l connection system that was developed in the STORT project. In the in-situ joining process, the shell and the bracket parts are combined in the C/C condition to create one integral part after the final RMI processing step as indicated in Figure 11. The single parts are prepared according to a standard method and a bonding agent is applied before the parts are combined in a fixture and siliconized thereafter to obtain an integral component. The flap parts make extensive use of the in-situ joining method. The individual flap components are made from plates by machining in the C/C condition and then joining them. Parts like the actuator rod were directly machined from C/C-SiC plates.

7. VERIFICATION

The design process of the TPS components included detailed numerical simulations to ensure the structural integrity of the system under the expected thermal-mechanical loads. The numerical verification process started with a transient thermal

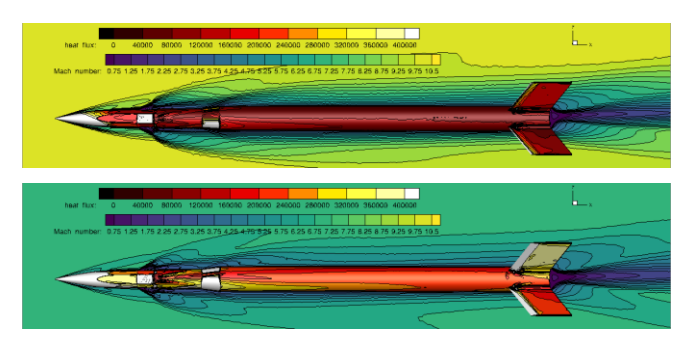


Figure 14 Example CFD solutions for the ATHEAt vehicle. (top: M=10 (ascent), bottom: M=7 (decent)). Temperatures are in K, heat flux in W/m².

analysis, which was followed by a mechanical analysis for the time points with the most critical load combinations.

As the basis for the thermal analysis, CFD simulations using the spacecraft version of the DLR code TAU[10] were performed. For the flight trajectory non-equilibrium effects are minor and air was treated as being in chemical equilibrium. Two example field and surface solutions are shown in Figure 14. These simulations provide the distribution of heat flux and pressure over the whole vehicle for selected flight times at the most important conditions.

In addition, with an in-house simplified tool the transient heat load was estimated for the whole flight based on an analytical approach. Furthermore, as the two methods gave the cold-wall heat flux, the hot-wall heat flux was calculated using an iterative approach. By combining the analytical results with the CFD results, and scaling for the hot-wall heat flux, the detailed distributions over the entire vehicle surface were made useful for transient calculations at every desired time step.

As an example, thermal analysis results obtained for the tip and the segment A section will be presented in brief. This will also explain one of the specific design problems encountered in the tip. In addition, it highlights how the chosen trajectory path is reflected in the surface temperatures of the vehicle. To give a comparison, the measured temperatures from the STORT flight are presented in [9].

The variation of the heat flux over the vehicle length is considerable. The very high values of the stagnation region quickly decrease when positions downstream are considered. In Figure 15 the cold-wall heat flux distributions for various flight conditions are shown. In the stagnation region, the CFD simulation predicts values of up to 20 MW/m², however, the y-axis of the plot is limited to 2.5 MW/m² to present the relevant data for the surface of the tip and segment A.

As mentioned, the cold-wall heat flux was transformed into hot-wall data. The transient hot-wall heat flux for the stagnation region is shown in Figure 16. It can be noted that the heat flux rises very sharply from almost zero to a high value of more than 5 MW/m² in the stagnation region at the

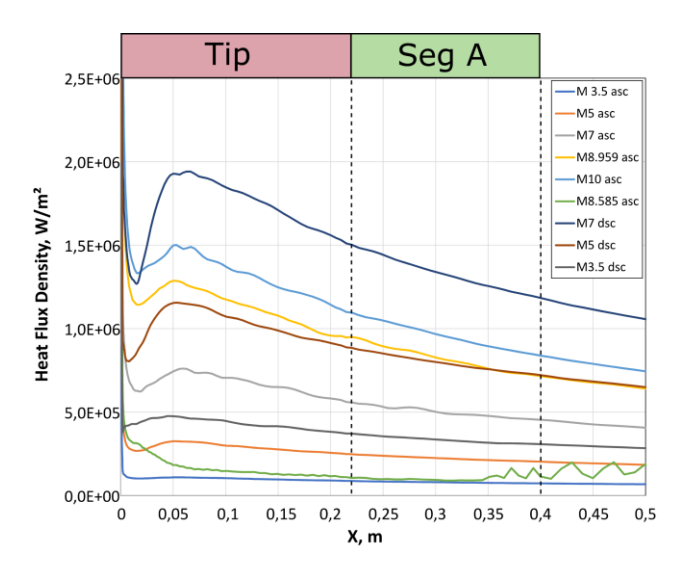


Figure 15 Cold-wall heat flux distribution over the length of the forebody for various flight conditions.

flight time of 79 s as a result of the second stage velocity increase. It decreases as sharply to be followed by a phase of high heat flux until a second peak is reached around 240 s where the heat flux value is over 3 MW/m². Towards the end of the flight, as the velocity decreases rapidly and the convective cooling in the lower atmosphere becomes dominant, there is negative hot-wall heat flux.

The heat flux profiles over time for different x-positions are also displayed in Figure 16. The last x-position is the front end of the segment A structures at 220 mm distance from the stagnation point. It can be noted that the heat flux is much lower there, always below 1 MW/m².

Using this data, the transient thermal analysis was performed. For the tip thermal analysis results are shown in Figure 17. The temperature distribution in the tip as the result of the transient hot-wall heat flux is shown at characteristic times. On top in Figure 17 a) the temperature at the time of 79 s into the flight is displayed, which is the time of the maximum velocity where the first heat flux peak in Figure 16 is experienced. The maximum temperature in the stagnation region of the tip is very high, with a predicted value of over 2500 °C. However, it can be noted that, due to the short nature of the heat flux peak and the rather big mass of the component, the tip is not heating up much inside and towards the interface to segment A. In Figure 17 b) the temperature distribution at the time of 240 s is presented, at the time of the second heat flux peak.

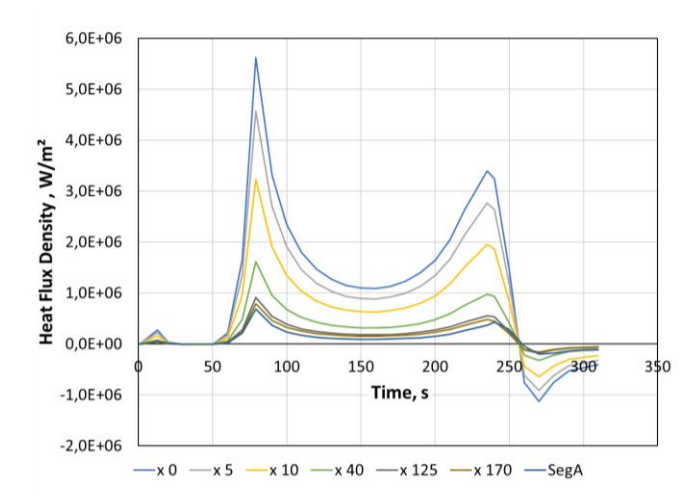


Figure 16 Hot wall heat flux at the tip.

The peak temperature on the tip is again very high at more than 2200 °C and, more important, also the temperature towards the interface to segment A has climbed to over 600 °C. This is important because the tip is connected directly to the metallic substructure of segment A via metallic fasteners. The detailed design of this connection is quite challenging and will be presented in another publication. After the second heat flux peak, the temperature in the stagnation region falls quickly, whereas in the center and rear of the tip the temperature remains high.

The surface temperature evolution on the segment A panels is a good example to show why the suppressed trajectory was chosen and how it affects the aerothermal environment. The temperature in the segment A CMC panel reaches a first maximum at 118 s and 991 °C, shown in Figure 18 a), which is considerably later than in the stagnation point of the tip.

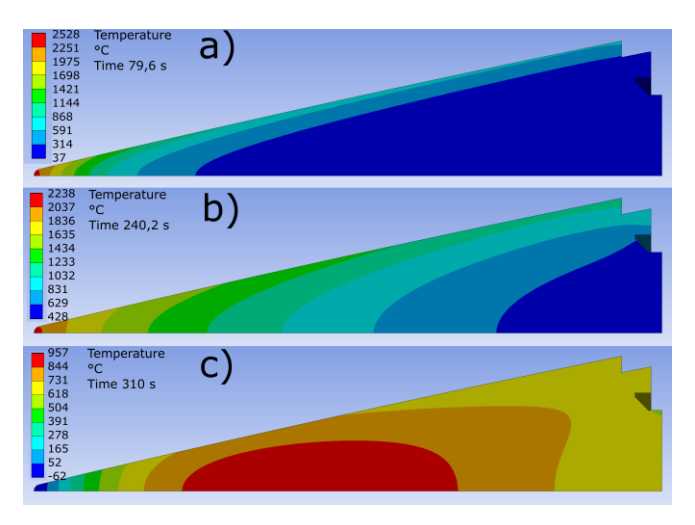


Figure 17 Temperatures in the tip at the characteristic times of a) 79 s, b) 240 s and c) 310 s.

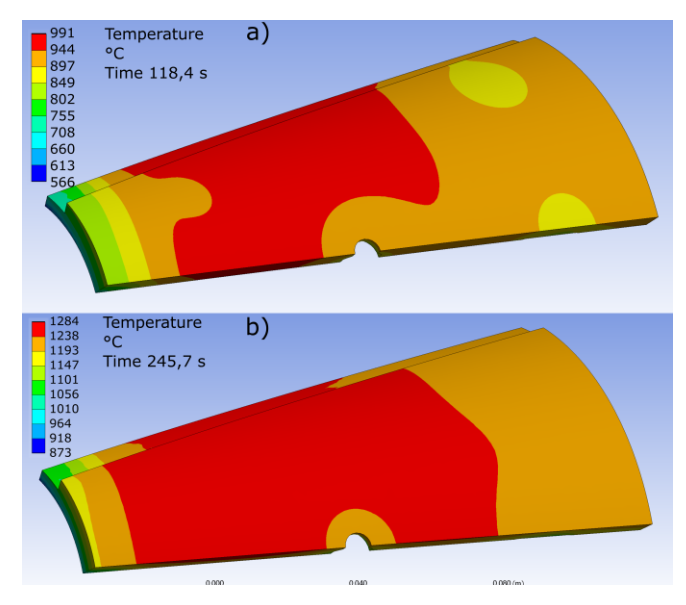


Figure 18 Temperature distribution on the CMC panel of segment A at the time of a) 118 s and b) 245 s.

But, thereafter the temperature stays almost constant for two minutes until it increases again with the second heat flux peak to reach 1284 °C at 245 s, shown in Figure 18 b). This is exactly what is intended with the suppressed trajectory, to keep the aerothermal loads fairly constant at a high value.

The time history of the segment A maximum temperature on the surface panel is shown in Figure 19. A critical element in the TPS design are the connections between CMC panels and the metallic substructure. Here, the double-l connection design as proven in STORT is used. It consists of two brackets, one which is made of CMC material and an integral part of the CMC panel, the second one is a metallic bracket that is connected to the CMC bracket and the metallic substructure via a bolt and nut connection.

The connection was validated for temperature and mechanical stress. To achieve acceptable conditions, the fastener and nut are made from a nickel alloy.

As the detailed TPS design process will be the topic of follow-on publications, it is mentioned just for completeness that the stresses in the CMC components are quite low in the shell structures. The design was in general driven by the connection elements, mostly the CMC brackets.

8. SENSORS

As the objective of the ATHEAt flight is to collect flight data under relevant environmental conditions, the TPS serves also as the placement position of the sensors that collect the aerothermal data. In this section, a brief overview is given of the suite of sensors that will be installed in the TPS.

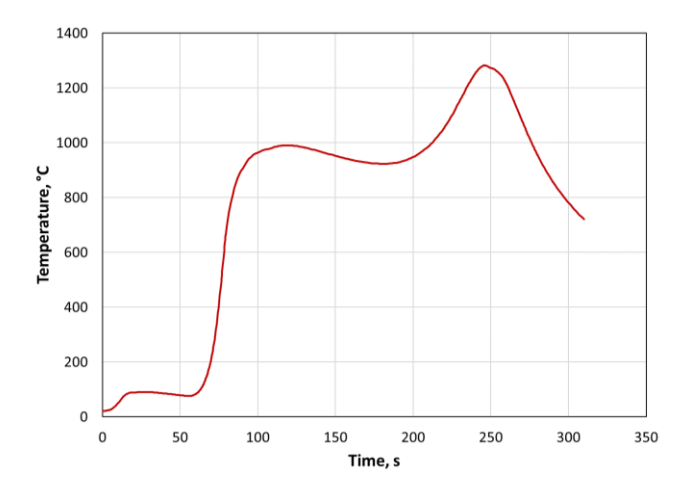


Figure 19 Maximum temperature on the Seg.A Panel.

The sensor types that are used in the TPS include the following: thermocouples, coaxial thermocouples (heat flux), pressure sensors, infrared cameras, pyrometers, laser displacement sensors (both point and line). The thermocouples are embedded in the CMC structure, either in boreholes or a slot in the material which is then filled with a filler material The coaxial thermocouples are placed directly in boreholes and are exposed to the outer surface.

The pressure measurement is done in two ways. In the tip, boreholes are machined into the structure and a metallic tube is connected to it to transmit the pressure to the sensor that is placed at a distance. In the shells, the pressure sensor is mounted on a CMC insert which is placed in the shell to keep the sensor at a safe distance from the surface.

Two types of laser displacement sensors are installed in several positions, both point and line sensors. The displacement measurement is of interest for the structural performance validation. The measurement is done on the inner side of the CMC surface structures and also on the CMC flap leeward side.

9. CONCLUSION

The ATHEAt flight experiment is a mission that will achieve high velocity between Mach 8 and Mach 10 for a considerable time of flight. This will generate high aerothermal loads in terms of heat flux and pressure and thus a robust TPS based on a thorough design layout is required. In addition, the TPS is the carrier structure for a large number of sensors to collect flight data. To meet both tasks, major development steps were made in comparison to the systems flown on STORT or previous vehicles.

The developed CMC structures represent a high quality standard with many improvements from the point of view of the material processing and also the structure layout. New manufacturing technologies were implemented with good results, concerning the wet filament winding technology and also the production of complex shaped integral shell

structures. In addition, with regard to the flaps, a hot structure kinematic system was added to investigate complex aerodynamic phenomena.

10. REFERENCES

- [1] H. Weihs, J. Longo and A. Gülhan, "The sharp edge flight experiment SHEFEX", 4th European Workshop on Hot Structures and TPS for Space Vehicles, Palermo, Italien, 26-29 November 2002.
- [2] H. Böhrk, H. Elsäßer, H. Weihs and M. Sippel, "The SHEFEX II Thermal Protection System," 7th European Symposium on Aerothermodynamics, Brugge, Belgium, ESA SP-692, p. 96.
- [3] A. Gülhan, D. Hargarten, M. Zurkaulen, F. Klingenberg, F. Siebe, S. Willems, G. Di Martino and T. Reimer, "Selected results of the hypersonic flight experiment STORT", Acta Astronautica, Volume 211, 2023, Pages 333-343, https://doi.org/10.1016/j.actaastro.2023.06.034..
- [4] G.D. Di Martino, T. Reimer, L. Dauth and L. Baier, "Structure Design of a Sounding Rocket Fairing with a Segmented Filament Winding-Ceramic Matrix Composite Thermal Protection System", 2nd International Conference on High-Speed Vehicle Science Technology, 2022, Bruges, Belgium.
- [5] T. Reimer, G. Di Martino, I. Petkov, L. Dauth, L. Baier and A. Gülhan, "Design, Manufacturing and Assembly of the STORT Hypersonic Flight Experiment Thermal Protection System", 25th AIAA International Space Planes and Hypersonic Systems and Technologies Conference, May 28-June 1, 2023, Bengaluru, Karnataka, India https://doi.org/10.2514/6.2023-3089
- [6] A. Gülhan, F. Klingenberg, S. Willems, D. Hargarten, J. Ettl, T. Reimer and L. Baier, "Long Duration Hypersonic Flight Experiment ATHEAT", 75th International Astronautical Congress, Milano, Italy, 2024, IAC-24,D2,6,6,x82390.
- [7] W. Krenkel, in "Ceramic Matrix Composites: Fiber Reinforced Ceramics and their Applications," Wiley & Sons, 2008, ISBN 3527622403
- [8] R. Kochendorfer, N. Lutzenburger and H. Weihs, "Joining Techniques for Fibre Ceramic Structures", Advanced Composites Letters, 13 (1) (2004),

doi: 10.1177/096369350401300106.

- [9] T. Reimer, G. Di Martino, L. Dauth, L. Baier, A. Gülhan, F. Klingenberg and D. Hargarten, STORT Hypersonic Flight Experiment Forebody Temperature Results, AIAA SCITECH 2025 Forum, 6-10 January, 2025, Orlando, FL https://doi.org/10.2514/6.2025-1342
- [10] S. Langer, A. Schwöppe and N. Kroll "The DLR Flow Solver TAU Status and Recent Algorithmic Developments", 52nd Aerospace Sciences Meeting, Jan 13-17, 2014, National Harbor, Maryland, USA